Limnol. Oceanogr., 57(3), 2012, 711–726

doi:10.4319/lo.2012.57.3.0711

Quantification of ammonia oxidation rates and ammonia-oxidizing archaea and bacteria at high resolution in the Gulf of California and eastern tropical North Pacific Ocean

J. Michael Beman,[a,b,*] Brian N. Popp,[b] and Susan E. Alford[a]

[a] School of Natural Sciences, University of California, Merced, California
[b] School of Ocean and Earth Science and Technology, University of Hawaii, Honolulu, Hawaii

Abstract

Ammonia-oxidizing microorganisms compete with phytoplankton for reduced nitrogen in the euphotic zone and provide oxidized nitrogen to other microbes present in the sea. We report $^{15}NH_4^+$ oxidation rate measurements made at 5–20-m resolution using an in situ array and quantification of ammonia-oxidizing archaea (AOA) and ammonia-oxidizing bacteria (AOB) in corresponding samples from the upper water column and oxygen minimum zone (OMZ) of the Gulf of California (GOC) and eastern tropical North Pacific Ocean (ETNP). $^{15}NH_4^+$ oxidation rates varied substantially with depth and between stations: they were greatest at the base of the euphotic zone, and maximum rates were up to 28-fold greater than rates measured within 5–10 m. Pyrosequencing and quantitative polymerase chain reactions (QPCR) indicated that AOA were present throughout the water column at all latitudes and always outnumbered AOB. AOB constituted only 39 of 432,240 16S ribosomal ribonucleic acid gene sequences produced via pyrosequencing but were more abundant at greater depths and higher latitudes. $^{15}NH_4^+$ oxidation rates were correlated with AOA abundance at some stations and were detectable in 96% of samples, including depths where oxygen concentrations were < 5 μmol kg^{-1} and depths within the euphotic zone, where up to 42% of ammonia oxidation occurred. Ammonia is rapidly oxidized within discrete depth intervals in the GOC and ETNP; while pyrosequencing and QPCR demonstrate that AOB are confined to deeper portions of the water column, AOA appear to be active within the euphotic zone, where they may quickly respond to nitrogen inputs.

Nitrification is a central process in the oceanic nitrogen (N) cycle that acts as a biogeochemical bridge between N inputs from the atmosphere via N_2 fixation and N losses via the anaerobic processes of denitrification and anaerobic ammonium oxidation (anammox) (Francis et al. 2007; Canfield et al. 2010*a*). Because N is a required nutrient for all organisms and limits primary production across large areas of the ocean (Mills et al. 2004), determining how nitrification may affect N availability is of critical importance. However, two emerging lines of research indicate that our understanding of oceanic nitrification is incomplete: nitrification is now thought to occur at higher rates and over greater depth ranges than previously appreciated (Yool et al. 2007; Church et al. 2010; Santoro et al. 2010), and marine *Thaumarchaeota* (Brochier-Armanet et al. 2008) play a substantial but poorly constrained role in nitrification (Agogue et al. 2008; Beman et al. 2008; Santoro et al. 2010). Because the cultivated marine thaumarchaeon *Nitrosopumilus maritimus* (Könneke et al. 2005) has a remarkable affinity for ammonia (NH_3) that would allow organisms with similar physiology to directly and successfully compete with phytoplankton for N (Martens-Habbena et al. 2009), placing quantitative constraints on nitrification rates and nitrifier distributions in the sea is essential to our understanding of oceanic N cycling.

The two sequential steps of nitrification are catalyzed by different groups of microorganisms: ammonia-oxidizing bacteria (AOB) and ammonia-oxidizing archaea (AOA) oxidize ammonia (NH_3) to nitrite (NO_2^-), and nitrite-oxidizing bacteria (NOB) subsequently oxidize NO_2^- to nitrate (NO_3^-); our focus in this study is the first and rate-limiting step of the process: ammonia oxidation. Coupled ammonia and nitrite oxidation consequently convert the most reduced form of N in the ocean (NH_3) to the most oxidized form (NO_3^-) such that the energy gained by AOA, AOB, and NOB must ultimately be expended by other organisms when they assimilate NO_2^- or NO_3^- (Raven 2009)—phytoplankton, for instance, must reduce NO_2^- or NO_3^- when these oxidized forms of N are incorporated for biosynthesis. Light is thought to inhibit nitrification, with ammonia oxidizers being less sensitive than NOB (reviewed by Lomas and Lipschultz 2006). However, nitrification can be detected in the euphotic zone (Wankel et al. 2007; Church et al. 2010; Santoro et al. 2010), indicating that nitrification occurs in the light. This also suggests that nitrifiers directly compete with phytoplankton for reduced N. In fact, Yool et al. (2007) combined published open ocean nitrification rate measurements (mostly using ^{15}N-labeled NH_4^+) with an intensive measurement program in the North Atlantic Ocean and found that specific nitrification rates (normalized to $[NH_4^+]$ and expressed as day^{-1}) were high in surface waters and showed little seasonality or variation with latitude. The major implication of this work was that estimates of the *f*-ratio (Eppley and Peterson 1979)—and hence carbon export—were significantly lower when accounting for near-surface nitrification. Yool and colleagues calculated that 25–30%

* Corresponding author: jmbeman@gmail.com

of all marine primary production (i.e., not just new production) is sustained by NO_3^- that is produced in the euphotic zone by nitrification. This surprising global-scale calculation is supported by direct measurements on a regional scale: Santoro et al. (2010) compared ^{14}C primary production rates with nitrification rates measured in the California Current and calculated that nitrification could supply 25–36% of the N required by phytoplankton.

A more important biogeochemical role for oceanic nitrification squares well with ammonia serving as an energy source for marine *Thaumarchaeota*: these organisms dominate microbial communities beneath the euphotic zone, where they number ~ 30% of all cells and constitute one of the most abundant microbial groups in the sea (Karner et al. 2001). Evidence for ammonia oxidation by marine *Thaumarchaeota* continues to accumulate, and with a few exceptions (Agogue et al. 2008; but *see* Konstantinidis et al. 2009; Church et al. 2010; Santoro et al. 2010), molecular studies indicate that many *Thaumarchaeota* have the ability to oxidize ammonia (i.e., are AOA; Francis et al. 2005) and actively do so in the ocean (Lam et al. 2007; Beman et al. 2008; Church et al. 2010). AOA outnumber AOB by several orders of magnitude in seawater (Mincer et al. 2007; Beman et al. 2008, 2010), but how these microbial groups vary in relation to one another and across oceanographic gradients is not well known.

Ammonia oxidation is particularly important in oceanic oxygen minimum zones (OMZs), where low oxygen conditions at depth allow N loss through anaerobic N cycling processes to occur. How exactly N cycling proceeds in these regions is debated (Lam et al. 2009; Ward et al. 2009; Canfield et al. 2010*b*) but has an important bearing on the global N cycle because OMZs are unequivocally areas of fixed N loss from the ocean. In OMZs, ammonia and nitrite oxidation provide a source of oxidized N compounds that may be used by denitrifiers or anammox bacteria as electron acceptors and converted to gaseous forms under anaerobic conditions (Lam et al. 2007, 2009; Canfield et al. 2010*a*). Ammonia oxidation is therefore a prerequisite for N loss in OMZs. Nitrogen loss subsequently starves these regions of fixed N (Beman et al. 2005; White et al. 2007), and N turns over rapidly in these regions (Ward and Zafiriou 1988; Lipschultz et al. 1990; Lam et al. 2009); hence, competition for N between high-affinity AOA and other organisms is likely to be intense. Adding to this complexity, OMZs are expanding as a consequence of climate change (Keeling et al. 2010), altering the rates and distribution of N transformations in the water column. Placing quantitative bounds on microbially driven biogeochemical processes occurring in OMZs is therefore essential.

Here we quantify ammonia oxidation rates and ammonia oxidizer distributions across an oceanographic transect through northern portions of the eastern tropical North Pacific Ocean (ETNP), the largest oceanic OMZ. Using an in situ floating array and stable isotope tracer, ammonia oxidation rates were measured at higher resolution with depth than in any previous study. Ammonia oxidizers were quantified using real-time quantitative polymerase chain reactions (QPCR) and next-generation pyrosequencing of bacterial communities, producing a detailed view of ammonia oxidation in this biogeochemically important region of the ocean.

Methods

Sampling—Samples were collected in July and August 2008 aboard the R/V *New Horizon*. Seven stations were occupied for several days each, and temperature, conductivity, and chlorophyll concentrations were measured using a Seabird SBE 9 conductivity-temperature-depth (CTD) sensor package equipped with a Seapoint fluorometer and photosynthetically active radiation sensor (Biospherical Instruments QSP-2300). Samples were collected using 10-liter PVC bottles deployed on the CTD rosette; samples for nutrient measurements and Winkler titrations were typically collected on the first cast and analyzed within hours of collection to characterize the structure of the water column. We selected depths for rate measurements and collection of deoxyribonucleic acid (DNA) samples based primarily on nutrient concentrations: one to three depths above the primary NO_2^- and NH_4^+ maxima were targeted, followed by five to seven depths spaced every 5 m and several additional depths spaced every 10–20 m. At each of these depths, ammonia oxidation rates were measured via addition of ^{15}N-labeled NH_4^+ to polycarbonate sample bottles deployed on a free-floating array (*see* below), and DNA samples were collected (*see* below). Water samples for rate measurements and DNA samples were collected on the same cast at all stations. These were collected 14–20 h following nutrient/Winkler samples at Sta. 1–6; at Sta. 7, nutrient and oxygen samples were collected 4 h after the rate and DNA samples.

Biogeochemical measurements—Oxygen concentrations were measured using a SBE oxygen sensor and corrected based on Winkler titrations ($r^2 = 0.997$ for 187 samples for the cruise). Winkler-corrected SBE oxygen data are shown for the casts where rate and DNA samples were collected. NH_4^+ concentrations were measured using the fluorometric method of Holmes et al. (1999), and NO_2^- and NO_3^- concentrations were measured using standard colorimetric techniques (Strickland and Parsons 1972); NO_3^- was reduced to NO_2^- with cadmium for measurement. Samples collected at depths greater than 100 m were frozen and analyzed at the College of Oceanic and Atmospheric Sciences at Oregon State University following the cruise. A subset of samples that were measured aboard ship was included in this analysis, and shore-based analyses agreed well with shipboard measurements ($r^2 = 0.88$) but were slightly lower in concentration. Hence, frozen samples were corrected to shipboard-measured concentrations; r^2 for standard curves were 0.996–0.999 (oxygen measurements), 0.959–0.999 (NH_4^+ measurements), and 0.993–0.999 (NO_2^- and NO_3^- measurements).

In situ free-floating array—To measure ammonia oxidation rates as accurately as possible under in situ conditions, we deployed a free-floating array with sample bottles suspended at multiple depths in the water column. The design of the free-floating array and the procedure used for

its deployment and recovery followed that described by Prahl et al. (2005). Water samples were collected from the rosette into 250-mL polycarbonate bottles in the dark using silicone tubing, and samples were overfilled by three volumes to avoid oxygen contamination; chilled ^{15}N-labeled NH_4Cl (*see* below) was quickly added via a 1-mL pipette, and the bottles were sealed. Bottles were attached to the array immediately before deployment at dawn, and the array was deployed for ~ 24 h under in situ temperature and light conditions. Our deepest array-based incubations were placed at 160-m depth, and samples collected from depths greater than 160 m were incubated at 12°C onboard the ship using temperature-controlled incubators; this includes nine samples reported here. For five suboxic samples (Sta. 2, 100 m; Sta. 3, 100 and 120 m; and Sta. 4, 140 and 160 m), duplicate incubations were conducted both on the array and onboard the ship in 125-mL Wheaton serum bottles sealed with Viton stoppers to minimize oxygen exposure. Following array recovery, samples were filtered through 0.2-μm syringe filters, collected in 50-mL high-density polyethylene bottles, and frozen at −20°C until analysis at the University of Hawaii.

$^{15}NH_4^+$ oxidation rate measurements—Ammonia oxidation rates were measured by adding 99 atom percent (at%) $^{15}NH_4^+$ to a concentration of 42 nmol L^{-1} and measuring the accumulation of ^{15}N label in the oxidized $NO_2^- + NO_3^-$ pool after incubation for ~ 24 h (Ward 2008). The $\delta^{15}N$ value of N_2O produced from $NO_2^- + NO_3^-$ using the "denitrifier method" (Sigman et al. 2001) was measured using methods described in Popp et al. (1995) and Dore et al. (1998). Briefly, N_2O produced from $NO_2^- + NO_3^-$ was transferred from a reaction vial, cryofocused, separated from other gases using a 0.32-mm-inner-diameter × 25-m PoraPLOT-Q capillary column (Agilent Technologies) at room temperature, and introduced into an ion source MAT252 mass spectrometer through a modified interface. Isotopic reference materials (United States Geological Survey-32, National Institute of Standards and Technology-3, University of Hawaii $NaNO_3$) bracketed every 12–16 samples and $\delta^{15}N$ values measured online were linearly correlated (r^2 = 0.996–0.999) with accepted reference material $\delta^{15}N$ values. Coefficients of variation for duplicate samples using this method ranged from 0.9% to 4.1% based on 41% of samples analyzed in duplicate. Accuracy and precision were further evaluated by multiple analyses of a sodium nitrate solution for which the $\delta^{15}N$ value of the solid $NaNO_3$ (i.e., University of Hawaii $NaNO_3$) had been previously determined using an online carbon-nitrogen analyzer coupled with an isotope ratio mass spectrometer (ConFlo II Delta-Plus) and were found to be less than ± 0.5‰ (± 0.00018 at% ^{15}N) for samples containing > 2.5 nanomoles of nitrate.

Initial at% enrichment of the substrate at the beginning of the experiment ($no\,NH_4^+$; *see* Eq. 1) was calculated by isotope mass balance based on NH_4^+ concentrations determined fluorometrically (Holmes et al. 1999) assuming that the ^{15}N activity of unlabeled NH_4^+ was 0.3663 at% ^{15}N. Rates of ammonia oxidation ($^{15}R_{ox}$) were calculated using an equation modified from Ward et al. (1989*b*):

$$^{15}R_{ox} = \frac{(n_t - no\mathrm{NO_x^-}) \times [\mathrm{NO_3^-} + \mathrm{NO_2^-}]}{(n\mathrm{NH_4^+} - no\mathrm{NH_4^+}) \times t} \quad (1)$$

where n_t is the at% ^{15}N in the $NO_3^- + NO_2^-$ pool measured at time t, $no\mathrm{NO_x^-}$, is the measured at% ^{15}N of unlabeled $NO_3^- + NO_2^-$, $no\mathrm{NH_4^+}$ is the initial at% enrichment of NH_4^+ at the beginning of the experiment, $n\mathrm{NH_4^+}$ is at% ^{15}N of NH_4^+ at time t, and $[NO_3^- + NO_2^-]$ is the concentration of the NO_x^- pool. We assume that ^{15}N enrichment of the substrate changed negligibly in the open ocean waters we examined (Kanda et al. 1987). Integrated rates of $^{15}NH_4^+$ oxidation were calculated on the basis of the average rates measured per depth interval above the rate peak and by integrating a fitted (power law) curve from the rate peak down through the water column.

^{13}C uptake measurements—Carbon uptake rates were measured using ^{13}C-labeled bicarbonate tracer at each sampling station. Water was transferred from rosette bottles into ~ 2-liter, acid-cleaned (10% HCl), and Milli-Q-rinsed polycarbonate bottles using acid-washed and sterilized silicone tubing; for each incubation depth, duplicate ~ 2-liter volumes were collected for determination of the ambient (time-zero) $\delta^{13}C$ value of particles and volumetric concentrations of particulate organic carbon and nitrogen. To each bottle, 0.25 mL of a 0.05 molar $NaH^{13}CO_3$ (99 atom% ^{13}C, Cambridge Isotope Laboratories) solution were added using a plunger-type syringe. All incubation bottles were filled to overflowing before being sealed with a Teflon-lined butyl rubber septum cap. Sample bottles were gently mixed, attached to the array, and deployed for ~ 24 h as described above. At the end of each incubation period, suspended particles were collected by gentle vacuum filtration through a 25-mm precombusted glass-fiber filter (450°C for 12 h, Whatman GF/F, nominal pore size 0.7 μm). Filters were immediately frozen (−20°C) until analysis. Samples were acid fumed, dried overnight at 60°C, and then encapsulated in tin cups prior to analysis of their carbon isotopic composition using the methodology described in Prahl et al. (2005). Based on previous experience in the Gulf of California, a 15% dark correction was applied to all calculations of ^{13}C uptake rates (White et al. 2007).

DNA sample collection and extraction—Two liters of seawater were collected from the CTD rosette and filtered through 25-mm-diameter 0.2-μm Suppor filters (Pall Corporation) using a peristaltic pump. Filters were flash frozen in liquid nitrogen and then stored at −80°C until DNA extraction using a protocol slightly modified from Beman et al. (2008): filters were bead beat for 2 min and then incubated with 800 μL of lysis buffer (20 mmol L^{-1} EDTA, 400 mmol L^{-1} NaCl, 750 mmol L^{-1} sucrose, 50 mmol L^{-1} Tris) and 100 μL of 10% SDS at 99°C for 1 min using a dry heat block; following the addition of 100 μL of proteinase K (10 mg mL^{-1}), samples were incubated at 55°C for 3 h. Lysates were purified using Qiagen DNeasy columns according the manufacturer's protocol (Qiagen), and DNA concentrations were mea-

Table 1. Details of QPCR assays used in this study. Includes primers used (and reference), cycling conditions, standards used, range of r^2 values for standard curves from different QPCR runs, and efficiency range for different runs.

Assay	Primers (reference)	Cycling conditions	QPCR standard	r^2	Efficiency
Archaeal *amoA*	Arch-amoAF and Arch-amoAR (Francis et al. 2005)	95°C (4 min); 30 × 95°C (30 s), 53°C (45 s), 72°C (60 s with detection step); dissociation curve	Clone GOC-G-60-9 (GenBank accession no. EU340472) dilution series	0.986–0.999	86.6–100%
MG1 *Crenarchaeota* 16S rRNA	GI_741F and GI_956R (Mincer et al. 2007)	95°C (4 min); 30 × 94°C (15 s), 58°C (30 s), 72°C (30 s), detection step at 78°C (7 s); dissociation curve	Clone arc11april01.150 dilution series	0.953–0.992	96.0–114%
Betaproteobacterial *amoA*	amoAF and amoA2R (Rotthauwe et al. 1997)	95°C (5 min); 40 × of 94°C (45 s), 56°C (30 s), 72°C (60 s), detection step at 81°C (7 s); dissociation curve	Clone HB_A_0206_G01 (GenBank accession no. EU155190) dilution series	0.968–0.998	82.9–100%

sured using the PicoGreen assay and the manufacturer's protocol (Life Technologies Corporation).

QPCR analyses—QPCR analyses were identical to those used by Beman et al. (2010). Archaeal *amoA* and 16S ribosomal ribonucleic acid (rRNA) QPCR assays used the following reaction chemistry: 12.5 μL of SYBR Premix F (Epicentre Biotechnologies), 2 mmol L^{-1} $MgCl_2$, 0.4 μmol L^{-1} of each primer, 1.25 units of AmpliTaq polymerase (Life Technologies Corporation), 40 ng μL^{-1} bovine serum albumin (Life Technologies Corporation), and 1 ng DNA in a final volume of 25 μL. βAOB were quantified using the same reaction chemistry but without additional $MgCl_2$. Primers (and relevant references for primer sequences), cycling conditions, QPCR standards, standard curve correlation coefficients, and PCR efficiencies are listed in Table 1. All QPCR assays were performed on a Stratagene MX3005P QPCR system (Agilent Technologies), and continuity among QPCR assays was maintained by including in each run a subset of samples (n = 6–8) from the previous run.

Pyrosequencing—DNA samples collected at all depths at Sta. 1–6 were sequenced using Titanium chemistry on the Roche 454 FLX platform at Research and Testing Laboratories. No samples from Sta. 7 were sequenced. We used the Bacteria-specific primers 27F (5′-GAGTTTGATCNTGGCTCAG-3′) and 519R (5′-GWNTTACNGCGGCKGCTG-3′) (Engelbrektson et al. 2010) modified with additional degeneracies (Ns in primer sequence)

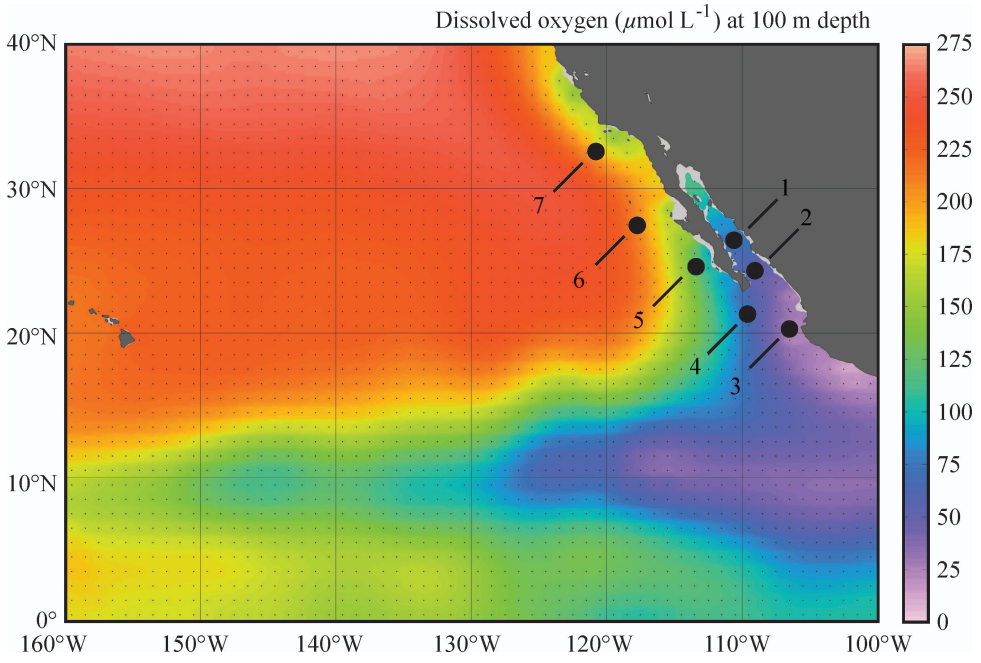

Fig. 1. Cruise track in the GOC and ETNP. Station locations are plotted on dissolved oxygen concentrations (μmol L^{-1}) at 100-m depth from the World Ocean Atlas in Ocean Data View.

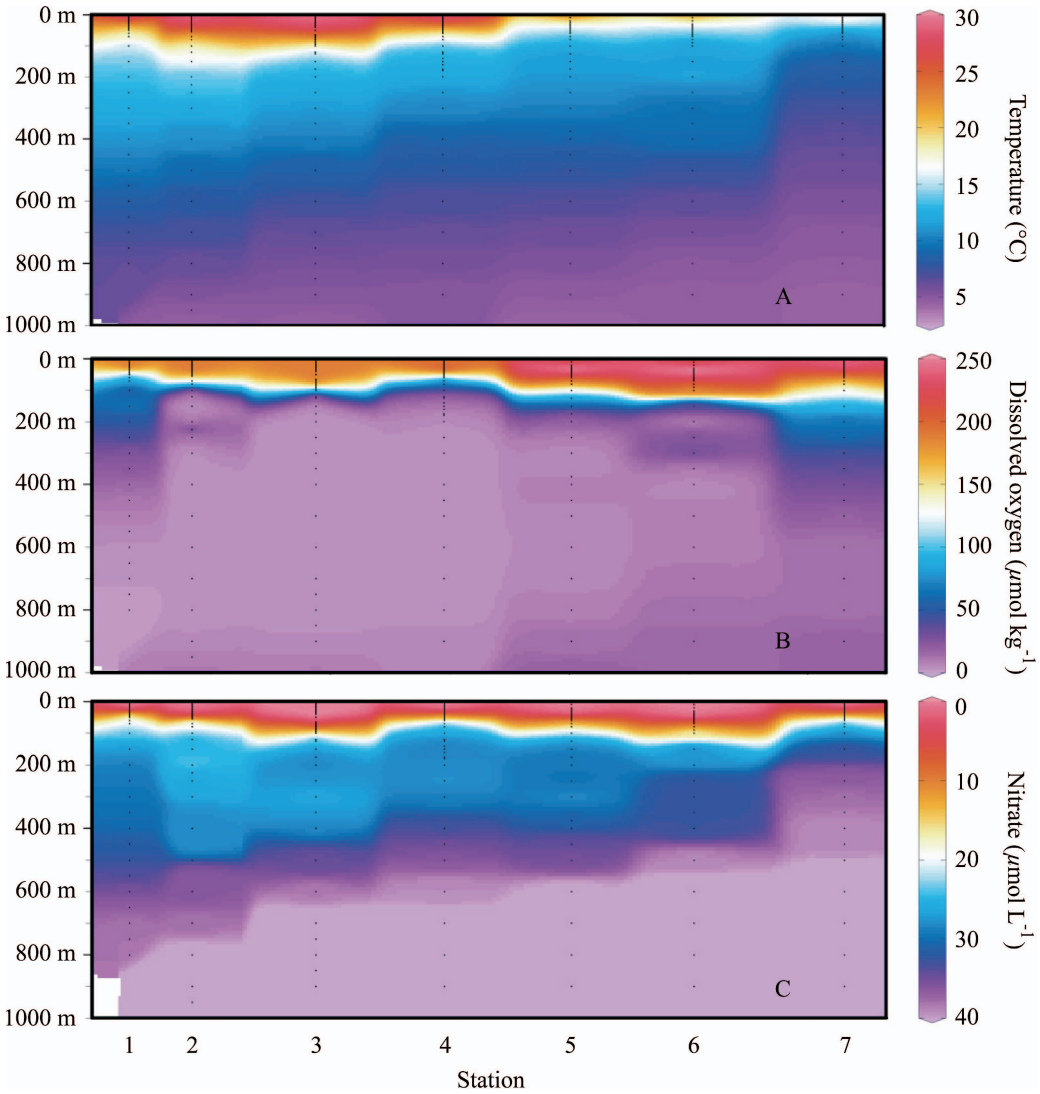

Fig. 2. Sections of (A) temperature (°C), (B) dissolved oxygen concentrations (μmol kg^{-1}), and (C) nitrate concentrations (μmol L^{-1}) along the cruise track. Location of stations is indicated along the horizontal axis; vertical axes display depths down to 1000 m. Small black dots denote the depths of bottle samples collected for nitrate measurements, and discrete temperature and oxygen data for the same depths were extracted from the CTD data. Data were gridded in Ocean Data View.

to amplify a portion of the bacterial 16S rRNA gene. Relevant Roche linkers were attached to primers, as were eight-base "bar codes" (Hamady et al. 2008) used to sort 60 individual samples from the six stations. For the 60 samples, we recovered 714,245 sequences with a median read length of 475 base pairs (bp).

For quality control, we used the approach of Huse et al. (2007) that is commonly used in the literature (Brown et al. 2009; Galand et al. 2009). Briefly, we used the program mothur (http://www.mothur.org; Schloss et al. 2009) to discard sequences: $> \pm 100$ bp from the median sequence length, containing any ambiguous bases, containing homopolymers > 8 bp, of < 25 average quality score, and that did not exactly match the forward primer and bar code sequence. The final criterion is where most (62% of all discarded sequences) sequences were removed. We did not screen sequences based on the reverse primer, as some of the reads are high-quality sequences that did not extend to the reverse primer. In total, 282,005 sequences (34%) did not meet quality control criteria and were excluded from subsequent analyses; a total of 432,240 bacterial 16S rRNA sequences were analyzed. Community composition of individual samples was determined using the Ribosomal Database Project Classifier (http://pyro.cme.msu.edu; Wang et al. 2007) using default parameters. Kunin et al. (2010) note that pyrosequencing errors may inflate estimates of microbial diversity, but our analysis is insensitive to this, as we are identifying AOB sequences based on similarity to database sequences. AOB 16S rRNA sequence data have been submitted to the GenBank database under accession numbers JQ478836-JQ478874.

Data analysis—Oceanographic data were visualized in Ocean Data View (http://odv.awi.de), and statistical analyses were conducted in MATLAB version 7.6.0 (R2008a).

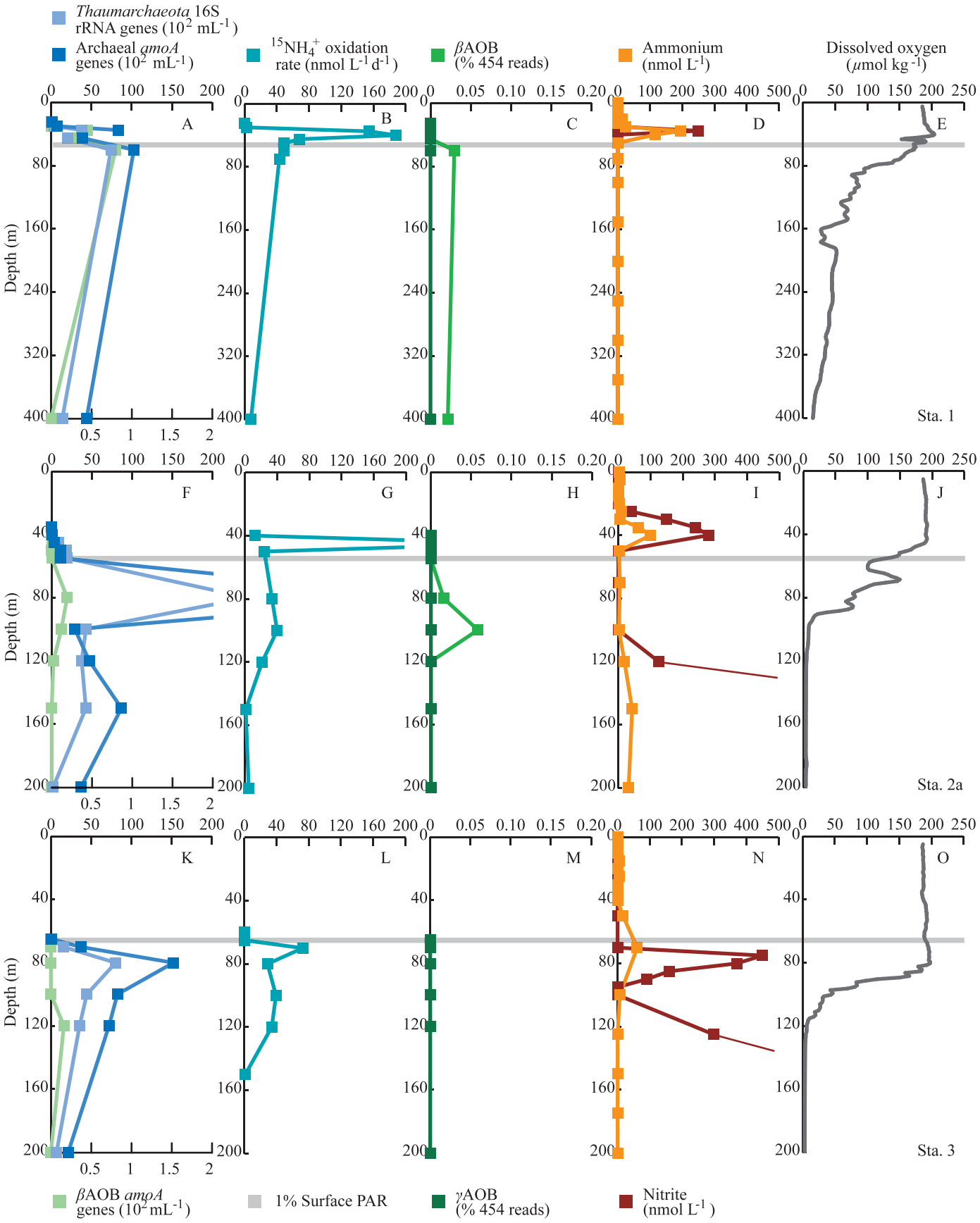
Thaumarchaeota 16S rRNA genes (10^2 mL^-1)
Archaeal amoA genes (10^2 mL^-1)
15NH4+ oxidation rate (nmol L^-1 d^-1)
βAOB (% 454 reads)
Ammonium (nmol L^-1)
Dissolved oxygen (μmol kg^-1)
Depth (m)
A
B
C
D
E
Sta. 1
F
G
H
I
J
Sta. 2a
K
L
M
N
O
Sta. 3
βAOB amoA genes (10^2 mL^-1)
1% Surface PAR
γAOB (% 454 reads)
Nitrite (nmol L^-1)

Results

Oceanographic variability in oxygen and nutrient concentrations—The OMZ of the ETNP extends from the west coast of Mexico and Central America halfway across the Pacific Ocean (Fig. 1). Suboxic waters reach their most northerly position off the coast of Baja California Sur, where at 24.7°N dissolved oxygen concentrations are 5–10 μmol kg^{-1} from 250 to 800 m. Low oxygen waters also extend into the Gulf of California (GOC) and reach similar latitudes (Figs. 1, 2B). In July 2008, we sampled a series of seven stations in the ETNP and GOC that spanned this oxygen gradient: Sta. 1 was located in the Carmen Basin of the GOC, Sta. 2 was located near the mouth of the GOC, and Sta. 3 was located in the core of the ETNP OMZ (Fig. 1), where oxygen concentrations declined rapidly with depth and dropped to 5 μmol kg^{-1} by 120 m (Fig. 2B). Four additional stations extended north from the tip of Baja California Sur (Sta. 4) to several hundred kilometers off the coast of San Diego, California (Sta. 7; Fig. 1). Sta. 2 was sampled twice (referred to as 2a and 2b in the text). Along this transect, sea surface temperatures declined strongly from south to north, reaching nearly 30°C at Sta. 3 and less than 18°C at Sta. 7 (32.5°N; Fig. 2A). Dissolved oxygen (DO) concentrations exhibited several broad trends, including minimum absolute concentrations of < 3 μmol kg^{-1} measured at Sta. 3, the southernmost station, as well as shoaling of the oxycline and thickening of the suboxic water mass to the south (Fig. 2B). Suboxic waters (DO < 5 μmol kg^{-1}) extended from 560 to 900 m at Sta. 1, from 120 to 915 m at Sta. 2a (with an intrusion of water with higher oxygen concentrations at 220–255 m), from 125 to 895 m at Sta. 3, from 175 to 875 m at Sta. 4, and from 304 to 330 m and 510 to 565 m at Sta. 5. DO exceeded 5 μmol kg^{-1} at all depths at Sta. 6 and 7 (Fig. 2B).

The depth of the nitracline was greater at Sta. 3 and 6 (where NO_3^- was first detected at 75 and 55 m, respectively) but was relatively shallow at Sta. 1, 4, and 7, where NO_3^- was detectable at 25–40-m depth (Fig. 2C). We observed similar variation in NH_4^+ and NO_2^- concentrations between stations, but in contrast to NO_3^-, both reached maximum concentrations at discrete depths in the water column (Figs. 3D,I,N, 4D,I,N, 5C,G). NH_4^+ concentrations ranged from 5 to 195 nmol L^{-1} and peaked at 30–70-m depth in primary NH_4^+ maxima. At Sta. 6, NH_4^+ was rarely detected throughout the water column (detection limit was 5 nmol L^{-1}), which may be indicative of rapid uptake, oxidation, or both (Fig. 4N). At Sta. 2a, NH_4^+ concentrations were slightly elevated at 150–200 m, corresponding with the top of the OMZ (DO concentrations drop below 5 μmol kg^{-1} at 105 m). NO_2^- concentration exhibited primary maxima at similar depths to NH_4^+, but the primary nitrite maximum (PNM) was offset from the NH_4^+ maximum by 5–10 m at Sta. 3, 4, and 7 and was colocated with the NH_4^+ maximum at Sta. 1, 2a, and 5 (Figs. 3D,I,N, 4D,I,N, 5C,G). Prominent secondary nitrite maxima were also observed at Sta. 2 and 3 in OMZ waters: NO_2^- concentrations at these depths were an order of magnitude greater than in the PNM (up to 4.18 μmol L^{-1} at Sta. 2 and 4.24 μmol L^{-1} at Sta. 3; data not shown) and are evidence of NO_3^- reduction to NO_2^- under suboxic conditions (Lipschultz et al. 1990; Lam et al. 2009; Ward et al. 2009). This feature extended from ~ 100 to 400 m at Sta. 3.

Variation in $^{15}NH_4^+$ oxidation rates—Accumulation of NH_4^+ in discrete subsurface maxima near the base of the euphotic zone is a result of remineralization of sinking organic material. Because NH_3 is used as a substrate by AOA and AOB and NO_2^- is the product of ammonia oxidation, we expected to find maximum $^{15}NH_4^+$ oxidation rates occurring at or near these depths and targeted them for highly resolved in situ array-based measurements. In fact, $^{15}NH_4^+$ oxidation occurred most rapidly within 0–30 m of the NH_4^+ and NO_2^- maxima at Sta. 1–6 (Figs. 3B,G,L, 4B,G,L). The maximum rate of $^{15}NH_4^+$ oxidation occurred 30 m below the PNM at Sta. 7, but we did not make measurements within the PNM (Fig. 5F,G). Hence, rate profiles showed a similar pattern to nutrient profiles: rates were low (although often detectable) at depths above the PNM, were highest near the PNM, and eventually declined with increasing depth in the water column.

$^{15}NH_4^+$ oxidation rates ranged from 0 to 348 nmol L^{-1} d^{-1} across different depths and stations in the GOC and ETNP (Figs. 3B,G,L, 4B,G,L, 5B,F). The maximum rate of 348 nmol L^{-1} d^{-1} occurred at 45 m at Sta. 2a and was greater than most maximum ammonia oxidation rates reported in the literature, such as 288 nmol L^{-1} d^{-1} in the eastern tropical South Pacific (ETSP; Lipschultz et al. 1990), 283 nmol L^{-1} d^{-1} in the ETSP (Ward et al. 1989*a*), 262 nmol L^{-1} d^{-1} in the Benguela upwelling region (Rees et al. 2006), 210 nmol L^{-1} d^{-1} off central California (Santoro et al. 2010), and 137.4 nmol L^{-1} d^{-1} at Sta. ALOHA in the North Pacific Subtropical Gyre (Dore and Karl 1996). The only oceanic ammonia oxidation rate measurements that exceed the maximum rate measured in the GOC and ETNP were 4900 nmol L^{-1} d^{-1}, measured by Lam et al. (2009) in

←

Fig. 3. Data for (A–E) Sta. 1, (F–J) Sta. 2a, and (K–O) Sta. 3 in the ETNP and GOC. (A,F,K) QPCR data for *Thaumarchaeota*, AOA, and AOB (16S rRNA or *amoA* genes per mL); (B,G,L) $^{15}NH_4^+$ oxidation rates (in nmol L^{-1} d^{-1}); (C,H,M) pyrosequencing data for gamma- and beta-proteobacterial AOB (expressed as percentage of total 16S rRNA reads for a given sample); (D,I,N) ammonium and nitrite concentrations (nmol L^{-1}); and (E, J, O) dissolved oxygen concentrations (μmol kg^{-1}). The gray line denotes the depth of 1% SPAR. All data are plotted to 200-m depth, with the exception of Sta. 1 data, which are plotted to 400-m depth. Note that AOA and AOB QPCR data are plotted on separate axes in panels A, F, and K and that some rate data and nitrite data plot off scale at Sta. 2a and 3 (*see* main text).

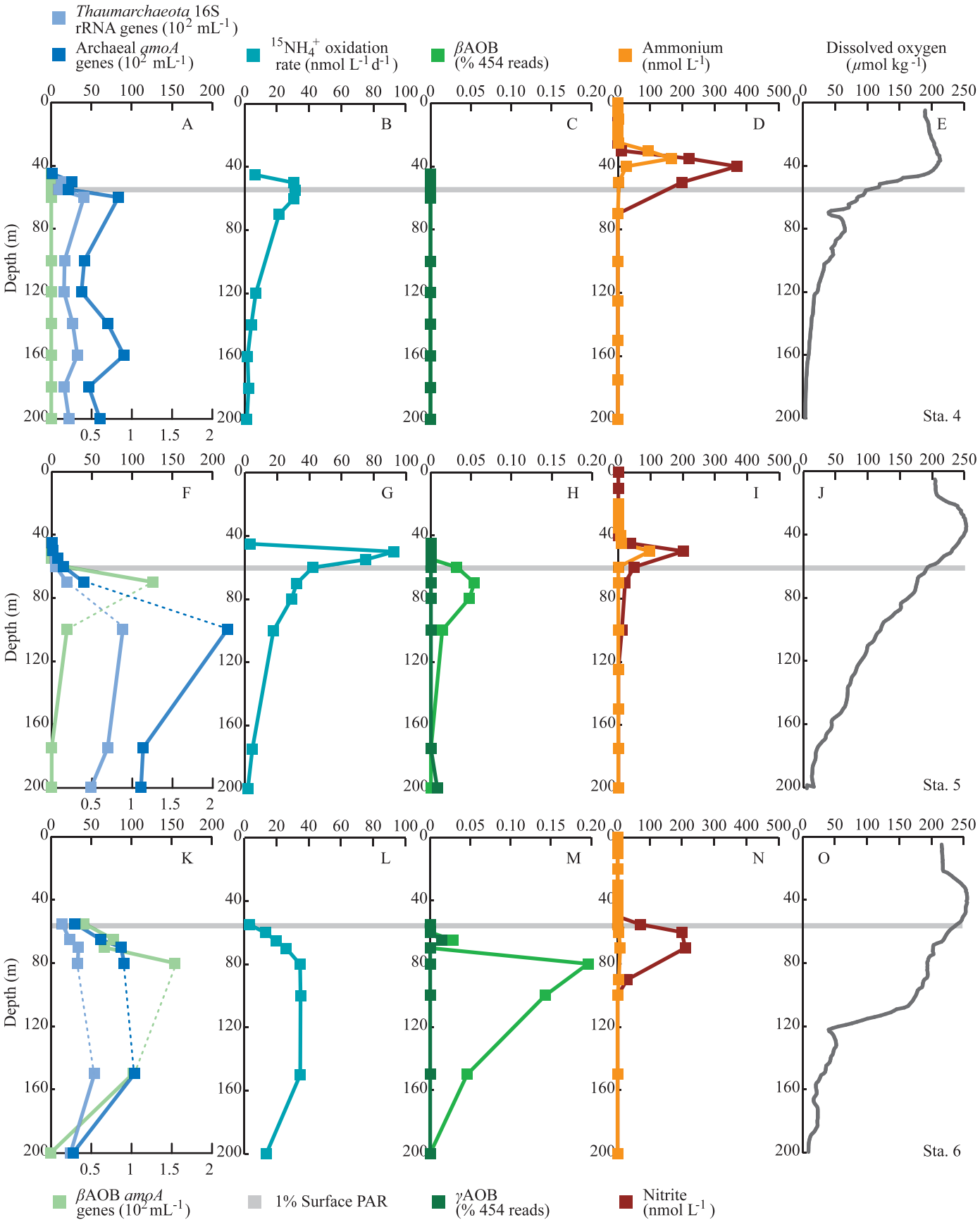
Thaumarchaeota 16S rRNA genes (10^2 mL^-1)
Archaeal amoA genes (10^2 mL^-1)
15NH4+ oxidation rate (nmol L^-1 d^-1)
βAOB (% 454 reads)
Ammonium (nmol L^-1)
Dissolved oxygen (μmol kg^-1)
Depth (m)
A
B
C
D
E
Sta. 4
F
G
H
I
J
Sta. 5
K
L
M
N
O
Sta. 6
βAOB amoA genes (10^2 mL^-1)
1% Surface PAR
γAOB (% 454 reads)
Nitrite (nmol L^-1)

the ETSP, and 1000 nmol L^{-1} d^{-1}, measured by Molina and Farias (2009), also in the ETSP. Our highest measured rate was also 14–28 times greater than those measured just 5 m above and below, at 40- and 50-m depth at Sta. 2a (Fig. 3G). This finding highlights the need for high-resolution measurements of nitrification rates in the water column, as pronounced peaks in $^{15}NH_4^+$ oxidation rates also occurred at Sta. 1 and, to a lesser degree, at Sta. 3–5. Rates at Sta. 1 ranged from 0 to 188 nmol L^{-1} d^{-1}, for example, with maximum rates of 154–188 nmol L^{-1} d^{-1} at 35–40 m that exceeded rates at 30 m (2 nmol L^{-1} d^{-1}) and 45 m (68.1 nmol L^{-1} d^{-1}). Coarse resolution measurements that miss these discrete peaks would obviously underestimate ammonia oxidation rates.

Ammonia oxidizer abundances and distributions—AOA and AOB abundances were quantified in tandem with $^{15}NH_4^+$ oxidation rate measurements, and QPCR measurements of 16S rRNA genes from marine *Thaumarchaeota* and archaeal ammonia mono-oxygenase subunit A (*amoA*) genes were strongly correlated with each other throughout the GOC and ETNP ($r^2 = 0.95$, $p < 0.001$). These data indicate that all *Thaumarchaeota* present in the GOC and ETNP, including those present under low-oxygen conditions, carry the *amoA* gene and therefore may be able to oxidize ammonia. These results contradict those produced using different *amoA* primer sets and that instead show a decrease in the ratio of *amoA*-containing *Thaumarchaeota* with depth (Agogue et al. 2008); however, the primers used in other studies likely miss some ''deep'' AOA ecotypes that have been detected in numerous other studies (*see* discussion in Konstantinidis et al. 2009; Santoro et al. 2010) and that all report strong correspondence between thaumarchaeal 16S rRNA and *amoA* genes (Church et al. 2010; Beman et al. 2010; Santoro et al. 2010).

AOA outnumbered betaproteobacterial AOB (βAOB) at every depth at every station by 5.5–15,300-fold. βAOB were quantified using a QPCR protocol specific for the bacterial *amoA* gene but were undetectable in most samples (Figs. 3A,F,K, 4A,F,K, 5A). However, we observed a general increase in βAOB abundance with increasing latitude: βAOB were not detected at Sta. 4, were present at low abundance at 120 m at Sta. 3 (16 *amoA* genes mL^{-1}; Fig. 3K), were slightly more abundant at Sta. 2a (0–22 *amoA* genes mL^{-1}; Fig. 3F), and increased in abundance from 0 to 126 *amoA* genes mL^{-1} at Sta. 1 and 5 (Figs. 3A,F), from 0 to 154 *amoA* genes mL^{-1} at Sta. 6 (Fig. 4K), and from 179 to 518 *amoA* genes mL^{-1} at Sta. 7 (Fig. 5E). βAOB were also present over an expanded range of depths at more northerly stations, from 60 to 100 m at Sta. 5, for example, and from 65 to 150 m at Sta. 6. At Sta. 6, AOA and AOB *amoA* genes were positively correlated ($r^2 = 0.71$, $p < 0.01$).

These findings were corroborated by pyrosequencing of bacterial 16S rRNA genes from all samples from Sta. 1–6. Out of 420,240 total sequences, only 33 were from βAOB, and only six gammaproteobacterial AOB (γAOB) sequences were detected (Table 3). AOB constituted just 0–0.1959% of reads in each library. The percentage of βAOB was correlated with *amoA* abundance measured using QPCR (Pearson's $r^2 = 0.59$, $p < 0.001$), and because the pyrosequencing libraries reflect the relative proportion of a given group within the bacterial assemblage (bacteria-specific 16S rRNA primers were used) while QPCR data measure abundances per unit volume, the correlation between QPCR and pyrosequencing data was stronger for the Spearman correlation (Spearman's $r^2 = 0.95$, $p < 0.001$). There were several instances where βAOB were detected at low levels using QPCR but were not present in pyrosequencing libraries; however, the opposite did not occur—AOB were always detectable via QPCR when present in the pyrosequencing libraries.

Pyrosequencing also allowed us to resolve individual clades of βAOB—*Nitrosomonas* and *Nitrosospira* sp.—and γAOB, such as *Nitrosococcus oceanii*; γAOB were rarely detected via pyrosequencing in the GOC and ETNP and were recovered only in libraries from 550 to 800 m at Sta. 1, 300 m at Sta. 2a, 160 m at Sta. 4, 200 m at Sta. 5, and 65 m at Sta. 6 (Table 3). This is consistent with low γAOB abundances reported in previous studies (Lam et al. 2007; Molina et al. 2007; Beman et al. 2008). The βAOB group *Nitrosomonas* was detected only at 80 and 100 m at Sta. 2a, whereas *Nitrosospira* sp. were detected at multiple depths at Sta. 1 and 2a and 5 and 6. The distribution of βAOB and γAOB 16S rRNA genes was also consistent within the water column, as *Nitrosospira* were typically present tens of meters below the PNM and just below the depth of 1% surface photosynthetically active radiation (SPAR; measured by CTD), while the γAOB *Nitrosococcus* were generally present at greater depths. The absolute abundance, the proportion of the bacterial community (based on pyrosequencing), and the depth range of AOB increased with latitude (Figs. 3A,C,F,H,K,M, 4A,C,F,H,K,M, 5A,E).

←

Fig. 4. Data for (A–E) Sta. 4, (F–J) Sta. 5, and (K–O) Sta. 6 in the ETNP and GOC. (A,F,K) QPCR data for *Thaumarchaeota*, AOA, and AOB (16S rRNA or *amoA* genes per mL); (B,G,L) $^{15}NH_4^+$ oxidation rates (in nmol L^{-1} d^{-1}); (C,H,M) pyrosequencing data for gamma- and beta-proteobacterial AOB expressed as percentage of total 16S rRNA reads for a given sample; (D,I,N) ammonium and nitrite concentrations (nmol L^{-1}); and (E,J,O) dissolved oxygen concentrations (μmol kg^{-1}). The gray line denotes the depth of 1% SPAR, and all data are plotted to 200-m depth. Note that AOA and AOB QPCR data are plotted on separate axes in panels A, F, and K and that $^{15}NH_4^+$ oxidation rates are plotted on axes with different ranges compared to those in Fig. 3 (100 vs. 200 nmol L^{-1} d^{-1}); ranges are identical for all other variables. Dashed lines connecting data points denote presence of DNA samples with QPCR inhibition that are subsequently excluded from statistical analyses.

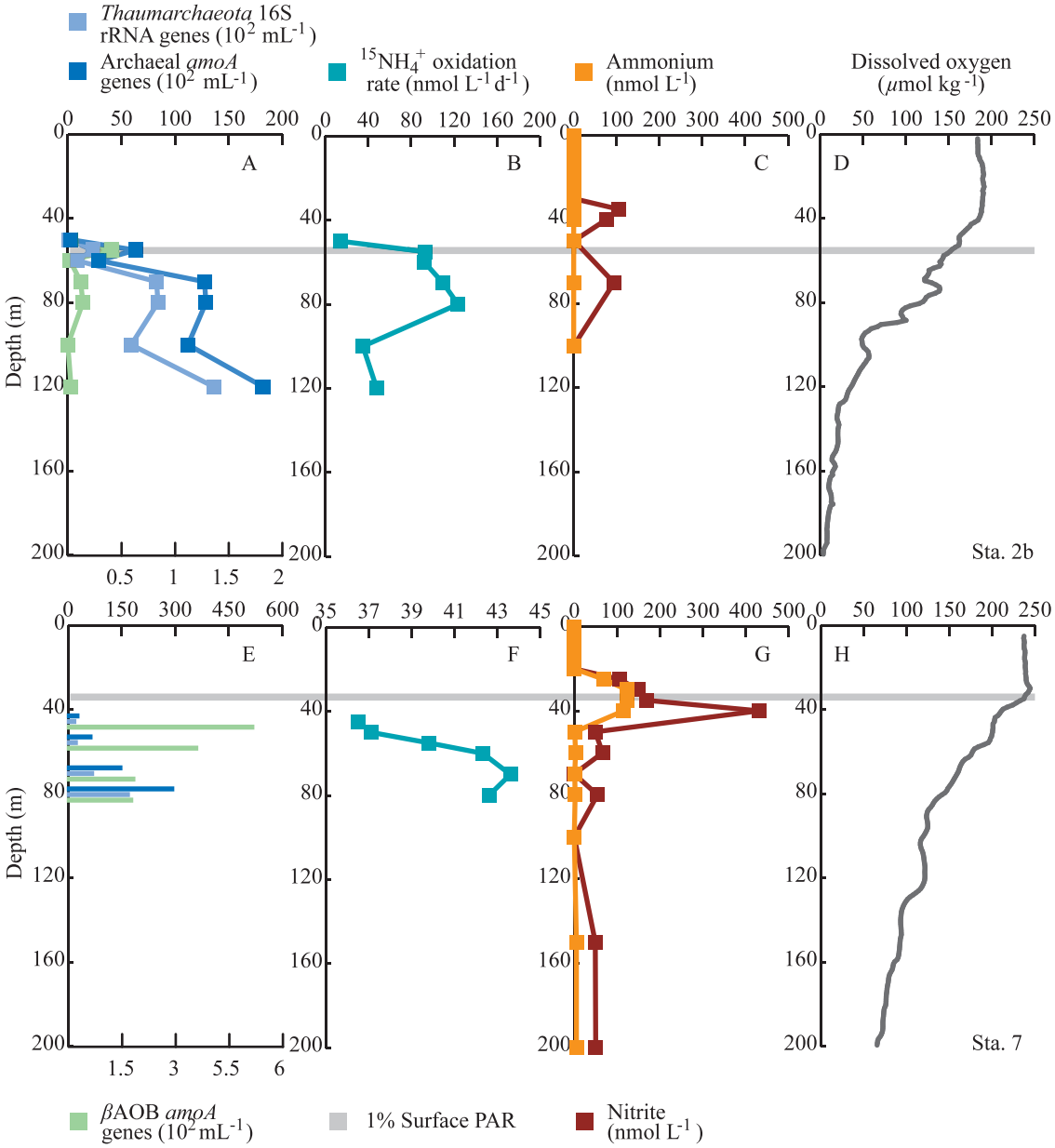

Fig. 5. Data for (E–H) Sta. 7 and the second sampling of (A–D) Sta. 2 in the ETNP and GOC. (A,E) QPCR data for *Thaumarchaeota*, AOA, and AOB (16S rRNA or *amoA* genes per mL); (B,F) $^{15}NH_4^+$ oxidation rates (in nmol L^{-1} d^{-1}); (C,G) ammonium and nitrite concentrations (nmol L^{-1}); and (D,H) dissolved oxygen concentrations (μmol kg^{-1}). Because of the limited QPCR data collected at Sta. 7, QPCR data are plotted as discrete data points rather than as a continuous depth profile. The gray line denotes the depth of 1% SPAR, and all data are plotted to 200-m depth. Note that AOA and AOB QPCR data are plotted on separate axes in panels A and E and that QPCR data and $^{15}NH_4^+$ oxidation rates from Sta. 7 are plotted on axes with different ranges compared to the other figures; ranges are identical for all other variables.

Discussion

AOA, AOB, and $^{15}NH_4^+$ oxidation rates—$^{15}NH_4^+$ oxidation rate profiles in the GOC and ETNP were characterized generally by low rates near the surface, peak rates near the PNM and NH_4^+ maximum at the base of the euphotic zone, and sharp decreases with depth that are typical of nitrification rates (Ward and Zafiriou 1988; Lipschultz et al. 1990; Ward 2008). Rate peaks were frequently offset from the PNM and ammonium maximum by several meters, however these maxima are generated via decoupling between NO_2^- and NH_4^+ supply and demand, and ammonia oxidation is one of several processes that produce and consume these compounds. NH_4^+ is generated by remineralization of sinking organic material and is assimilated by phytoplankton or oxidized; NO_2^- is produced by ammonia oxidation or through secretion by phytoplankton, and is then assimilated or oxidized. Formation of the PNM appears to be driven primarily by phytoplankton (reviewed by Lomas and Lipschultz 2006),

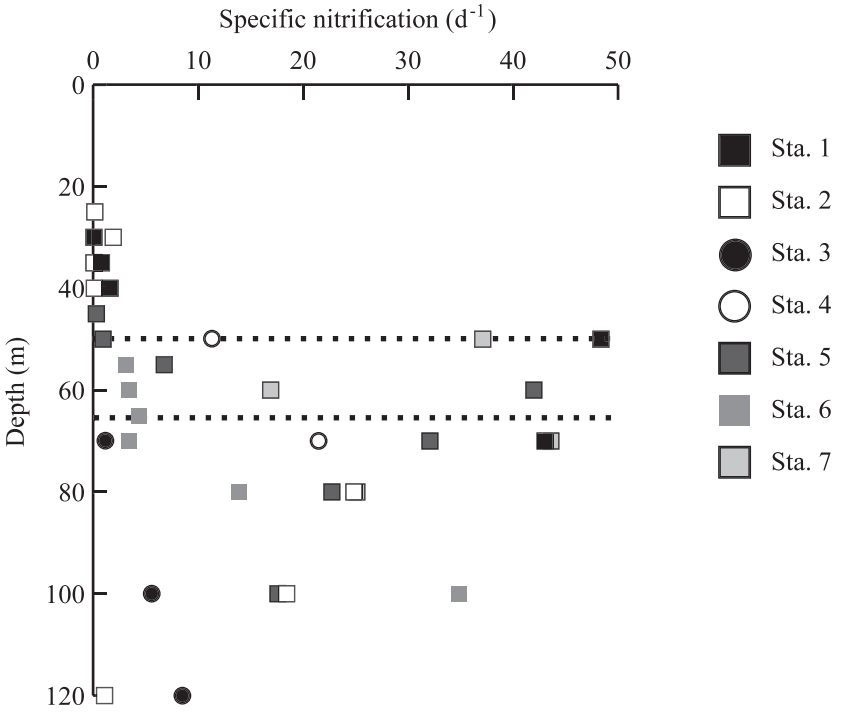

Fig. 6. Specific nitrification rates in the GOC and ETNP. Data from different stations are shown in shades of gray and with different symbols. Dashed lines denote 1% SPAR at Sta. 7 (50 m) and Sta. 3 (66 m); the depths of 1% SPAR at other stations fall between these values.

and our data are consistent with this, as the $^{15}NH_4^+$ oxidation rate maximum fell below the PNM at Sta. 2a, 2b, 4, 6, and 7, and rates were low within the PNM at these stations (Figs. 3–5). The rate maximum was 5 m above the PNM at Sta. 3, which likely reflects some combination of light limitation of phytoplankton, AOA/AOB, and NO_2^- oxidation. The rate peak and PNM were located at the same depth at Sta. 1 and 5, and it is possible that ammonia oxidation contributes to the formation of the PNM at these stations. $^{15}NH_4^+$ oxidation rates peaked within the ammonium maximum at Sta. 1, 3, and 5, suggesting that ammonia oxidizers quickly respond to regeneration of NH_4^+ at these stations. The rate maximum fell below the ammonium maximum at Sta. 2a, 4, and 7, but it is possible that ammonia oxidation in fact depletes NH_4^+ through rapid oxidation at these depths. Sta. 6 and 2b are good examples of this, as little NH_4^+ was present within the water column, and ammonia oxidation was active over a broad depth range (Figs. 4L,N, 5B,C).

Depth profiles of AOA based on *amoA* and 16S rRNA genes displayed a general pattern similar to $^{15}NH_4^+$ oxidation rates: *amoA* and 16S rRNA genes were absent or present only at low levels in the euphotic zone, reached a subsurface peak near the PNM, and then decreased with depth (Figs. 3A,F,K, 4A,F,K, 5A,E). This is consistent with AOA profiles collected off the coast of California (Santoro et al. 2010), in the equatorial Pacific Ocean (Church et al. 2010), and in the Black Sea (Lam et al. 2007). At some stations in the GOC and ETNP, rate and AOA profiles were similar, and ammonia oxidation rates and archaeal *amoA* genes were correlated with one another. The strongest correlation was observed at Sta. 6 ($r^2 = 0.88$, $p < 0.001$, for linear relationship; log $r^2 = 0.83$, $p < 0.002$, for logarithm of *amoA* genes), whereas rates and *amoA* genes were more weakly related at Sta. 1 (linear $r^2 = 0.43$, $p = 0.15$; $r^2 = 0.38$, $p > 0.05$, for log[*amoA*]), Sta. 3 (linear $r^2 = 0.24$, $p > 0.05$; $r^2 = 0.39$, $p = 0.07$, for log[*amoA*]), and Sta. 7 (linear $r^2 = 0.57$, $p > 0.05$; $r^2 = 0.84$, $p = 0.08$, for log[*amoA*]). At Sta. 4, rates and *amoA* were correlated in the upper 100 m of the water column (linear $r^2 = 0.34$, $p > 0.05$; $r^2 = 0.89$, $p = 0.06$, for log[*amoA*]). However, a subsurface peak in *amoA* genes, which occurred without a concurrent subsurface peak in rates, reduced the strength of the relationship throughout the water column (linear $r^2 = 0.043$, $p > 0.05$; $r^2 = 0.001$, $p > 0.05$, for log[*amoA*]).

Sta. 2a and 5 exhibited sharp peaks in oxidation rates within the euphotic zone, but AOA were most abundant 35–50 m below these rate peaks (Figs. 3F,G, 4F,G). Across our data set, rates were maximal, and AOA were most abundant (based on both 16S rRNA and *amoA*) at Sta. 2a, yet these peak values were separated by 35 m in the water column. Church et al. (2010) found high rates of *amoA* expression in the euphotic zone of the tropical and subtropical Pacific, including both high absolute levels of transcripts and elevated transcript abundances relative to gene copies. Although this may represent increased turnover of ammonia mono-oxygenase proteins due to damage (Church et al. 2010), our data—based on measurement of oxidation rates relative to gene abundances—also indicate relatively high per cell activity. Interestingly, identical measurements repeated at Sta. 2 8 d later produced different AOA and rate profiles (e.g.,

Table 2. Integrated ammonia oxidation rates and the proportion occurring within the euphotic zone compared with integrated carbon fixation rate. Integrated ammonia oxidation rates were calculated over the top 300 m of the water column, and the proportion occurring above 1% surface photosynthetically active radiation (SPAR) is expressed as a percentage of the total. Integrated carbon fixation rates are also shown. The proportion of N demand that is directly provided by nitrification in the euphotic zone is calculated on the basis of integrated carbon fixation rates and Redfield stoichiometry and expressed as percentage.

Sta.	Depth of 1% SPAR (m)	Integrated ammonia oxidation (mmol m^{-2} d^{-1})	% of integrated ammonia oxidation above 1% SPAR	Integrated carbon fixation (mmol m^{-2} d^{-1})	N provided by nitrification in euphotic zone (%)
1	56	7.7	33	67	25
2	55	4.6	42	34	37
3	66	2.3	1.6	31	0.77
4	56	1.4	19	27	6.4
5	57	3.0	29	47	12
6	60	4.9	1.5	30	1.6

maximum of 123 nmol L^{-1} d^{-1} at 80 m) as well as stronger correspondence between rates and *amoA* (r^2 = 0.46; Fig. 5A,B), suggesting that AOA respond rapidly to changing oceanographic conditions.

AOA have exceptional affinity for NH_3 and swiftly respond to pulses of N in pure culture (Martens-Habbena et al. 2009); we suggest that at Sta. 2 and 5 and in parts of the subtropical and tropical Pacific (Church et al. 2010), AOA rapidly metabolize newly available N, leading to high per cell oxidation rates and transcript abundances. Over time, increased NH_4^+ supply leads to elevated oxidation rates and allows AOA populations to expand and eventually approach steady state. This leads to the correspondence between rates and *amoA* observed at Sta. 1, 3, 6, and 7 and in the upper 100 m at Sta. 4. In support of this idea, per cell rates calculated from the slope of the regressions of $^{15}NH_4^+$ oxidation rates on thaumarchaeal 16S rRNA genes (assuming one copy of the 16S rRNA gene and excluding Sta. 2a and 5) yield values of 0.2–9.6 fmol $cell^{-1}$ d^{-1}. These values closely match those reported by Könneke et al. (2005) for *N. maritimus* (1.8–15.4 fmol $cell^{-1}$ d^{-1}). If this concept is correct, a testable hypothesis would be that AOA and oxidation rates are correlated in stratified or biogeochemically stable marine systems; calculated per cell rates would be more variable in physically disturbed systems or in areas where there is an influx of N due to lack of equilibration between population size and activity.

Oxygen, light, and $^{15}NH_4^+$ oxidation rates—Because N is regenerated while oxygen is depleted via microbial respiration of sinking organic material, ammonia oxidation rates are expected to closely parallel consumption of DO (Ward 2008). Nitrification may in fact directly contribute to

Table 3. Presence of 16S rRNA sequences from AOB in pyrosequencing data. For stations and sampling depths where AOB were detected, the total number of 16S rRNA sequences recovered is shown, as are total numbers of 16S rRNA sequences for the different of βAOB and γAOB genera *Nitrosospira*, *Nitrosomonas*, and *Nitrosococcus*. The sum of these is also expressed as a percentage of the total sequences for each sample. Note that no AOB were detected via pyrosequencing at Sta. 3 and 4.

Sta.	Depth (m)	Total bacterial 16S rRNA sequences	*Nitrosospira* βAOB 16S rRNA sequences	*Nitrosomonas* βAOB 16S rRNA sequences	*Nitrosococcus* γAOB 16S rRNA sequences	AOB (% of 16S rRNA sequences)
1	60	6749	2	0	0	0.0296
1	400	9285	2	0	0	0.0215
1	550	12,924	1	0	1	0.0155
1	700	6517	0	0	1	0.0153
1	750	8530	0	0	1	0.0117
1	800	8300	0	0	1	0.0120
2	80	5982	0	1	0	0.0167
2	100	6860	3	1	0	0.0583
2	250	5302	1	0	0	0.0189
5	60	6274	2	0	0	0.0318
5	70	3702	2	0	0	0.0540
5	80	8406	4	0	0	0.0476
5	100	7093	1	0	0	0.0141
5	200	12,627	0	0	1	0.0079
6	65	7193	2	0	1	0.0417
6	80	4084	8	0	0	0.1959
6	100	1400	2	0	0	0.1429
6	150	2192	1	0	0	0.0456
Total		432,240	31	2	6	0.0090

consumption of DO (Ward 2008), and assuming that DO concentrations and consumption are, to a first approximation, related to one another, we expect $^{15}NH_4^+$ oxidation rates to correlate with DO concentrations. Excluding shallow samples that had high oxygen concentrations but low rates (probably due to partial light limitation; *see* below), $^{15}NH_4^+$ oxidation rates were positively correlated with oxygen concentrations at Sta. 1–5 ($r^2 = 0.51$–0.98, all ANOVA $p < 0.05$). The slopes of these relationships differed from station to station, but this results from the fact that DO integrates consumption over long periods of time, whereas rate measurements capture the short-term response of microbial communities to N supply. Sta. 6 and 7 were characterized by broad $^{15}NH_4^+$ oxidation rate profiles where maximum rates were spread over tens of meters in the water column and were not correlated with DO. These maximum rates were also lower than those measured at other stations (Figs. 4L, 5F). The decay of ammonia oxidation with depth in the ocean demonstrates that it does not occur primarily on large, rapidly sinking particles (Ward 2008); hence, one possible explanation for the patterns observed at Sta. 6 and 7 is particle-based nitrification (Karl et al. 1984). While we did not specifically examine this, it is interesting in light of the increased abundance of AOB and the correlations between AOA, AOB, and rates observed at these stations (Figs. 3, 4). Here our data may capture a mix of particle-based and planktonic ammonia oxidation that is conducted by some combination of both AOA and AOB.

At both Sta. 2a and Sta. 3, a secondary rate peak occurred at 100 m on the edge of suboxic waters (Fig. 3G,L), and we frequently detected $^{15}NH_4^+$ oxidation down to DO concentrations of 4.1–8.5 μmol kg^{-1} in the GOC and ETNP. Rates were relatively low at these depths (due to low NH_4^+ flux), but suboxic nitrification has been observed before in both the ETNP (Ward and Zafiriou 1988) and the ETSP (Lipschultz et al. 1990). Exposure to atmospheric oxygen during sampling and processing was raised as a possible issue in previous studies (Ward and Zafiriou 1988) and could be a factor here, but Lipschultz et al. (1990) observed extremely high rates of $^{15}NH_4^+$ oxidation under low DO in the ETSP, and Ward and Zafiriou's (1998) results from the ETNP are similar to our own, as they observed positive correlation between DO and $^{15}NH_4^+$ oxidation rates (other than for euphotic zone samples). Shipboard measurements using sealed Wheaton vials did not differ significantly from parallel array-based measurements (ANOVA $p > 0.05$), indicating that oxygen contamination did not alter our measurements.

Substantial rates of ammonia oxidation were also measured within the euphotic zone in the GOC and ETNP. While our sampling approach specifically excluded euphotic zone samples at Sta. 3 and 6, our measurements were conducted under in situ light and temperature and were conducted above the level of 1% SPAR at Sta. 1, 2a, 4, and 5 (level of 1% SPAR indicated by gray line in Figs. 3,4). At these four stations, $^{15}NH_4^+$ oxidation was readily detected within the euphotic zone. Sta. 1, 2a, 4, and 5 also displayed detectable NH_4^+ above 1% SPAR, indicating that NH_4^+ is available for oxidation within the euphotic zone. It is not possible to use our data set to separate the effects of light and NH_4^+ supply on ammonia oxidation, but future work should address the interplay between light limitation and the availability of NH_4^+. We used our data to calculate integrated rates of ammonia oxidation over the top 300 m of the water column and found variation among stations of 1.38–7.72 mmol m^{-2} d^{-1} (Table 2)—values that are nearly identical to integrated rates of 1.13–2.76 mmol m^{-2} d^{-1} previously measured in the ETNP (Ward and Zafiriou 1988). Up to 42% of ammonia oxidation occurred within the euphotic zone (Sta. 2a), but this proportion was as little as 1.5–1.6% (based on limited measurements at Sta. 6 and 3) and was 19–33% at Sta. 1, 4, and 5 (Table 2). Integrated euphotic zone ammonia oxidation rates were also compared to integrated C uptake rates measured using ^{13}C-labeled bicarbonate. Based on Redfield C : N stoichiometry of $\sim$ 6.625, 0.8–37% of the N assimilated by phytoplankton may have been previously oxidized in the euphotic zone (Table 2). This is consistent with Santoro et al. (2010) in approach, and the proportion of N supplied by euphotic zone nitrification is similar (0.8–37% here vs. 25–36% in the California current), but our wider range of estimates results from in situ rate measurements that capture substantial variation in the depth distribution and magnitude of ammonia oxidation.

Following Yool et al. (2007), we calculated specific nitrification rates by dividing measured oxidation rates (in units of nmol L^{-1} d^{-1}) by NH_4^+ concentrations (in nmol L^{-1}), yielding units of d^{-1} (where NH_4^+ was undetectable, specific nitrification rates obviously could not be calculated). The highest specific rates measured in this study were up to 242-fold greater than the median value (0.2 d^{-1}) used by Yool et al. (2007), and 31 of 34 rate measurements were greater than 0.2 d^{-1} (Fig. 6). The lowest measured value was 0.08 d^{-1}. We found consistent variation in specific nitrification rates with depth: rates in the GOC and ETNP were generally low above 50 m but showed a sharp increase at 50 m at several stations and were elevated down to $\sim$ 100-m depth. Although estimates of N produced by euphotic zone nitrification as a proportion of phytoplankton N demand converge on $\sim$ 25–30% (Wankel et al. 2007; Yool et al. 2007; Santoro et al. 2010; Table 2), our results indicate that ammonia oxidation does not occur at uniform rates in the euphotic zone, as we consistently measured high rates at the bottom of euphotic zone. This variation could be an important factor in global estimates of nitrification and hence new production. A key point is that small changes in the depth of maximum nitrification relative to the depth of the euphotic zone can strongly affect the proportion of nitrification taking place within vs. below the euphotic zone (Table 2; Fig. 6). This may be important when considering the effects of warming-induced stratification, which may affect euphotic zone depth (Gruber 2011), and ocean acidification, which may displace nitrification downward (Beman et al. 2011), on the N cycle.

Methodological explanations for the discrete rate maxima that we observed include fluorometric measurements of NH_4^+ made at nmol L^{-1} concentrations, which increase measurement accuracy; rate measurements made at 5–20-m resolution with depth, increasing the chances of

capturing peaks in specific nitrification rates; and differences in sampling and experimental approaches that produce widely varying specific nitrification rates (e.g., *see* fig. 1b in Yool et al. 2007). However, many of the highest recorded ammonia oxidation rates have been measured in OMZ regions (although not within suboxic waters), including the ETSP (Ward et al. 1989*a*; Lipschultz et al. 1990; Lam et al. 2009), Benguela upwelling (Rees et al. 2006), and our measurements in the GOC and ETNP. Sutka et al. (2004) also measured an increase in nitrification rates as they transited from Sta. ALOHA in the North Pacific Subtropical Gyre into the ETNP but did not have sufficient depth resolution to identify rate peaks within the water column. While high ammonia oxidation rates have been observed at Sta. ALOHA (Dore and Karl 1996) and off the coast of California (Santoro et al. 2010), our results and those from earlier studies indicate that ammonia oxidation can be compressed into a relative thin layer in OMZs, where it occurs rapidly. This layer is found at the base of the euphotic zone, where sinking organic material is remineralized and NH_4^+ is regenerated, and is typically located within or just below the NH_4^+ maximum and within or just above the oxycline (Figs. 3–5). We hypothesize that these discrete rate maxima reflect increased ammonia supply in productive OMZ regions and the high ammonia affinity found among the AOA (Martens-Habbena et al. 2009), which together lead to rapid ammonia oxidation mediated by AOA.

Microbial oceanography of ammonia oxidation—These results are consistent with other researchers' work indicating that the AOA are important mediators of nitrification in the Black Sea (Lam et al. 2007), California Current (Santoro et al. 2010), and ETSP (Lam et al. 2009; Molina et al. 2010; Stewart et al. 2012) as well as our previous study of the GOC (Beman et al. 2008). In the metatranscriptomic analysis of Stewart et al. (2012), AOA dominated the transcriptome of the ETSP and represented one in five protein-coding transcripts at 85 m. Stewart et al. (2012) recovered few AOB transcripts, indicating that AOA were the dominant ammonia oxidizers in the ETSP. AOB were often undetectable by QPCR and pyrosequencing in the GOC and ETNP, including depths and stations where ammonia oxidation rates were substantial and AOA were present. For example, rapid $^{15}NH_4^+$ oxidation was measured in the euphotic zone, but no AOB were detected in thousands to tens of thousands of sequences. Combined with correspondence between $^{15}NH_4^+$ oxidation rates and MGI 16S rRNA and archaeal *amoA* genes, our results indicate that AOA actively oxidize ammonia in the ETNP.

However, our data also place constraints on the prospective niches of AOB within the ocean. They are consistent with light sensitivity in AOB (Lomas and Lipschultz 2006 and references therein), as AOB were not detected by either QPCR or pyrosequencing in the euphotic zone of the GOC and ETNP. At the greater depths where they were detected, AOB were located below AOA, and the few detectable γAOB were located below βAOB, leading to a "stratigraphy" of ammonia oxidizers in the water column. AOB sometimes exhibited a subsurface increase in abundance, including a clear increase at 80–100 m at Sta. 2a in association with a secondary peak in oxidation rates at the edge of the OMZ. In line with these findings, Lam et al. (2007) found that archaeal *amoA* transcripts were correlated with modeled ammonia oxidation rates in the Black Sea, but βAOB *amoA* was expressed at greater depths in the suboxic zone. In our data, AOB abundances were also correlated with oxidation rates at Sta. 6 ($r^2 = 0.77$, $p < 0.005$) and were more abundant at northern stations. Whether this reflects a large-scale pattern of increasing AOB abundance with increasing latitude will require additional measurements, but Church et al. (2010) observed a mirror-image pattern for AOA in the equatorial Pacific (specifically an increase in AOA abundance near the equator) suggestive of large-scale gradients in AOA and AOB throughout the Pacific Ocean.

Assembled together, our data capture rapid ammonia oxidation in the Gulf of California and ETNP that is variable with depth and among stations. *Thaumarchaeota* 16S rRNA genes and *amoA* genes were correlated with each other and with oxidation rates, whereas AOB were commonly undetectable by QPCR and among thousands of 16S rRNA sequences, supporting the idea that archaeal nitrification plays an important role in oceanic N cycling. It is also clear that AOA oxidize ammonia within the euphotic zone throughout the Pacific Ocean (Figs. 3, 4; Church et al. 2010; Santoro et al. 2010) and that oxidized N can be produced at substantial levels compared to phytoplankton N demand (Table 2; Dore and Karl 1996; Yool et al. 2007; Santoro et al. 2010). AOA may directly compete with phytoplankton for N throughout the upper ocean, while ammonia and nitrite oxidation supply oxidized N to anaerobic processes in OMZs; this coupling and competition among multiple processes and microbial groups yields a complicated N cycle that is still understudied (Lam et al. 2009; Ward et al. 2009; Canfield et al. 2010*b*) but must be understood in an ocean undergoing rapid change (Hutchins et al. 2009; Beman et al. 2011; Gruber 2011).

Acknowledgments

We are indebted to Rachel Foster for supplying critical nucleic acid samples, Angel White for calculating integrated carbon uptake rates, and Matt Meyerhof for compiling nitrification rate data from the literature. We thank Fred Prahl (chief scientist), Jackie Mueller, Natalie Walsgrove, Jason Smith, Julie Fliegler, and the officers and crew of the R/V *New Horizon* for assistance in the field; we also thank Chris Francis for fruitful conversations and thank Jackie Mueller, Natalie Walsgrove, C. J. Bradley, and Elizabeth Gier for assistance with laboratory analyses. This work was supported by National Science Foundation Oceanography (OCE) awards 08-24997 and 10-34943 to J.M.B. and B.N.P. This is School of Ocean and Earth Science and Technology Contribution number 8549.

References

Agogue, H., M. Brink, J. Dinasquet, and G. J. Herndl. 2008. Major gradients in putatively nitrifying and non-nitrifying Archaea in the deep North Atlantic. Nature **456:** 788–791, doi:10.1038/nature07535

Beman, J. M., K. R. Arrigo, and P. A. Matson. 2005. Agricultural runoff fuels large phytoplankton blooms in

vulnerable areas of the ocean. Nature **434:** 211–214, doi:10.1038/nature03370

———, B. N. Popp, and C. A. Francis. 2008. Molecular and biogeochemical evidence for ammonia oxidation by marine *Crenarchaeota* in the Gulf of California. ISME J. **2:** 429–441, doi:10.1038/ismej.2007.118

———, R. Sachdeva, and J. A. Fuhrman. 2010. Population ecology of nitrifying Archaea and Bacteria in the Southern California Bight. Environ. Microbiol. **12:** 1282–1292, doi:10.1111/j.1462-2920.2010.02172.x

———, and others. 2011. Global declines in oceanic nitrification rates as a consequence of ocean acidification. Proc. Natl. Acad. Sci. USA **108:** 208–213, doi:10.1073/pnas.1011053108

Brochier-Armanet, C., B. Boussau, S. Gribaldo, and P. Forterre. 2008. Mesophilic crenarchaeota: Proposal for a third archaeal phylum, the *Thaumarchaeota*. Nat. Rev. Microbiol. **6:** 245–252, doi:10.1038/nrmicro1852

Brown, M. V., and others. 2009. Microbial community structure in the North Pacific Ocean. ISME J. **3:** 1374–1386, doi:10.1038/ismej.2009.86

Canfield, D. E., A. N. Glazer, and P. G. Falkowski. 2010*a*. The evolution and future of Earth's nitrogen cycle. Science **330:** 192–196, doi:10.1126/science.1186120

———, and others. 2010*b*. A cryptic sulfur cycle in oxygen-minimum–zone waters off the Chilean coast. Science **330:** 1375–1378, doi:10.1126/science.1196889

Church, M. J., B. Wai, D. M. Karl, and E. F. DeLong. 2010. Abundances of crenarchaeal *amoA* genes and transcripts in the Pacific Ocean. Environ. Microbiol. **12:** 679–688, doi:10.1111/j.1462-2920.2009.02108.x

Dore, J. E., and D. M. Karl. 1996. Nitrification in the euphotic zone as a source of nitrite, nitrate and nitrous oxide at Station ALOHA. Limnol. Oceanogr. **41:** 1619–1628, doi:10.4319/lo.1996.41.8.1619

———, B. N. Popp, D. M. Karl, and F. J. Sansone. 1998. A large source of atmospheric nitrous oxide from subtropical North Pacific surface waters. Nature **396:** 63–66, doi:10.1038/23921

Engelbrektson, A., V. Kunin, K. C. Wrighton, N. Zvenigorodsky, F. Chen, H. Ochman, and P. Hugenholtz. 2010. Experimental factors affecting PCR-based estimates of microbial species richness and evenness. ISME J **4:** 642–647, doi:10.1038/ismej.2009.153

Eppley, R. W., and B. J. Peterson. 1979. Particulate organic matter flux and planktonic new production in the deep ocean. Nature **282:** 677, doi:10.1038/282677a0

Francis, C. A., J. M. Beman, and M. M. M. Kuypers. 2007. New processes and players in the nitrogen cycle: The microbial ecology of anaerobic and archaeal ammonia oxidation. ISME J. **1:** 19–27, doi:10.1038/ismej.2007.8

———, K. J. Roberts, J. M. Beman, A. E. Santoro, and B. B. Oakley. 2005. Ubiquity and diversity of ammonia-oxidizing archaea in water columns and sediments of the ocean. Proc. Natl. Acad. Sci. USA **102:** 14683–14688, doi:10.1073/pnas.0506625102

Galand, P. E., E. O. Casamayor, D. L. Kirchman, and C. Lovejoy. 2009. Ecology of the rare microbial biosphere of the Arctic Ocean. Proc. Natl. Acad. Sci. USA **106:** 22427–22432, doi:10.1073/pnas.0908284106

Gruber, N. 2011. Warming up, turning sour, losing breath: Ocean biogeochemistry under global change. Phil. Trans. R. Soc. A **369:** 1980–1996, doi:10.1098/rsta.2011.0003

Hamady, M., J. J. Walker, J. K. Harris, N. J. Gold, and R. Knight. 2008. Error-correcting barcoded primers for pyrosequencing hundreds of samples in multiplex. Nat. Methods **5:** 235–237, doi:10.1038/nmeth.1184

Holmes, R. M., A. Aminot, R. Kérouel, B. A. Hooker, and B. J. Peterson. 1999. A simple and precise method for measuring ammonium in marine and freshwater ecosystems. Can. J. Fish. Aquat. Sci. **56:** 1801–1808.

Huse, S., J. Huber, H. Morrison, M. Sogin, and D. Welch. 2007. Accuracy and quality of massively parallel DNA pyrosequencing. Genome Biol. **8:** R143, doi:10.1186/gb-2007-8-7-r143

Hutchins, D. A., M. R. Mulholland, and F. Fu. 2009. Nutrient cycles and marine microbes in a CO_2-enriched ocean. Oceanography **22:** 128–145, doi:10.5670/oceanog.2009.103

Kanda, J., E. A. Laws, T. Saino, and A. Hattori. 1987. An evaluation of isotope dilution effect from conventional data sets of ^{15}N uptake experiments. J. Plankton Res. **9:** 79–90, doi:10.1093/plankt/9.1.79

Karl, D. M., G. A. Knauer, J. H. Martin, and B. B. Ward. 1984. Bacterial chemolithotrophy in the ocean is associated with sinking particles. Nature **309:** 54–56, doi:10.1038/309054a0

Karner, M. B., E. F. DeLong, and D. M. Karl. 2001. Archaeal dominance in the mesopelagic zone of the Pacific Ocean. Nature **409:** 507–510, doi:10.1038/35054051

Keeling, R. F., A. Körtzinger, and N. Gruber. 2010. Ocean deoxygenation in a warming world. Annu. Rev. Mar. Sci. **2:** 199–229, doi:10.1146/annurev.marine.010908.163855

Könneke, M., A. E. Bernhard, J. R. de la Torre, C. B. Walker, J. B. Waterbury, and D. A. Stahl. 2005. Isolation of an autotrophic ammonia-oxidizing marine archaeon. Nature **437:** 543–546, doi:10.1038/nature03911

Konstantinidis, K. T., J. Braff, D. M. Karl, and E. F. DeLong. 2009. Comparative metagenomic analysis of a microbial community residing at a depth of 4,000 meters at Station ALOHA in the North Pacific Subtropical Gyre. Appl. Environ. Microbiol. **75:** 5345–5355, doi:10.1128/AEM.00473-09

Kunin, V., A. Engelbrektson, H. Ochman, and P. Hugenholtz. 2010. Wrinkles in the rare biosphere: Pyrosequencing errors can lead to artificial inflation of diversity estimates. Environ. Microbiol. **12:** 118–123, doi:10.1111/j.1462-2920.2009.02051.x

Lam, P., and others. 2007. Linking crenarchaeal and bacterial nitrification to anammox in the Black Sea. Proc. Natl. Acad. Sci. USA **104:** 7104–7109, doi:10.1073/pnas.0611081104

———, and ———. 2009. Revising the nitrogen cycle in the Peruvian oxygen minimum zone. Proc. Natl. Acad. Sci. USA **106:** 4752–4757, doi:10.1073/pnas.0812444106

Lipschultz, F., S. C. Wofsy, B. B. Ward, L. A. Codispoti, G. E. Friederich, and J. W. Elkins. 1990. Bacterial transformations of inorganic nitrogen in the oxygen-deficient waters of the eastern tropical South Pacific Ocean. Deep-Sea Res. A **37:** 1513–1541, doi:10.1016/0198-0149(90)90060-9

Lomas, M. W., and F. Lipschultz. 2006. Forming the primary nitrite maximum: nitrifiers or phytoplankton? Limnol. Oceanogr. **51:** 2453–2467, doi:10.4319/lo.2006.51.5.2453

Martens-Habbena, W., P. M. Berube, H. Urakawa, J. R. de la Torre, and D. A. Stahl. 2009. Ammonia oxidation kinetics determine niche separation of nitrifying Archaea and Bacteria. Nature **461:** 976–979, doi:10.1038/nature08465

Mills, M. M., C. Ridame, M. Davey, J. La Roche, and R. J. Gelder. 2004. Iron and phosphorus co-limit nitrogen fixation in the eastern tropical North Atlantic. Nature **429:** 292–294, doi:10.1038/nature02550

Mincer, T. J., M. J. Church, L. T. Taylor, C. M. Preston, D. M. Karl, and E. F. DeLong. 2007. Quantitative distribution of presumptive archaeal and bacterial nitrifiers in Monterey Bay and the North Pacific Subtropical Gyre. Environ. Microbiol. **9:** 1162–1175, doi:10.1111/j.1462-2920.2007.01239.x

Molina, V., L. Belmar, and O. Ulloa. 2010. High diversity of ammonia-oxidizing archaea in permanent and seasonal oxygen-deficient waters of the eastern South Pacific. Environ. Microbiol. **12:** 2450–2465, doi:10.1111/j.1462-2920.2010.02218.x

———, and L. Farías. 2009. Aerobic ammonium oxidation in the oxycline and oxygen minimum zone of the eastern tropical South Pacific off northern Chile (~20°S). Deep-Sea Res. II **56:** 1032–1041, doi:10.1016/j.dsr2.2008.09.006

———, O. Ulloa, L. Farias, H. Urrutia, S. Ramirez, P. Junier, and K. Witzel. 2007. Ammonia-oxidizing betaproteobacteria from the oxygen minimum zone off northern Chile. Appl. Environ. Microbiol. **73:** 3547–3555, doi:10.1128/AEM.02275-06

Popp, B. N., F. J. Sansone, T. M. Rust, and D. A. Merritt. 1995. Determination of concentration and carbon isotopic composition of dissolved methane in sediments and nearshore waters. Anal. Chem. **67:** 405–411, doi:10.1021/ac00098a028

Prahl, F. G., B. N. Popp, D. M. Karl, and M. A. Sparrow. 2005. Ecology and biogeochemistry of alkenone production at subtropical North Pacific Station ALOHA. Deep-Sea Res. I **52:** 699–719, doi:10.1016/j.dsr.2004.12.001

Raven, J. A. 2009. Contributions of anoxygenic and oxygenic phototrophy and chemolithotrophy to carbon and oxygen fluxes in aquatic environments. Aquat. Microb. Ecol. **56:** 177–192, doi:10.3354/ame01315

Rees, A. P., E. M. S. Woodward, and I. Joint. 2006. Concentrations and uptake of nitrate and ammonium in the Atlantic Ocean between 60°N and 50°S. Deep-Sea Res. II **53:** 1649–1665, doi:10.1016/j.dsr2.2006.05.008

Rotthauwe, J. H., K. P. Witzel, and W. Liesack. 1997. The ammonia monooxygenase structural gene *amoA* as a functional marker: molecular fine-scale analysis of natural ammonia-oxidizing populations. Appl. Environ. Microbiol. **63:** 4704–4712.

Santoro, A. E., K. L. Casciotti, and C. A. Francis. 2010. Activity, abundance and diversity of nitrifying archaea and bacteria in the central California Current. Environ. Microbiol. **12:** 1989–2006, doi:10.1111/j.1462-2920.2010.02205.x

Schloss, P. D., and others. 2009. Introducing mothur: Open-source, platform-independent, community-supported software for describing and comparing microbial communities. Appl. Environ. Microbiol. **75:** 7537–7541, doi:10.1128/AEM.01541-09

Sigman, D. M., K. L. Casciotti, M. Andreani, C. Barford, M. Galanter, and J. K. Böhlke. 2001. A bacterial method for the nitrogen isotopic analysis of nitrate in seawater and freshwater. Anal. Chem. **73:** 4145–4153, doi:10.1021/ac010088e

Stewart, F. J., O. Ulloa, and E. F. DeLong. 2012. Microbial metatranscriptomics in a permanent marine oxygen minimum zone. Environ. Microbiol. **14:** 23–40, doi:10.1111/j.1462-2920.2010.02400.x

Strickland, J. H., and T. R. Parsons. 1972. A practical handbook of seawater analysis, 2nd ed. Fisheries Research Board.

Sutka, R. L., N. E. Ostrom, P. H. Ostrom, and M. S. Phanikumar. 2004. Stable nitrogen isotope dynamics of dissolved nitrate in a transect from the North Pacific Subtropical Gyre to the eastern tropical North Pacific. Geochim. Cosmochim. Acta **68:** 517–527, doi:10.1016/S0016-7037(03)00483-6

Wang, Q., G. M. Garrity, J. M. Tiedje, and J. R. Cole. 2007. Naïve Bayesian classifier for rapid assignment of rRNA sequences into the new bacterial taxonomy. Appl. Environ. Microbiol. **73:** 5261–5267, doi:10.1128/AEM.00062-07

Wankel, S. D., C. Kendall, J. T. Pennington, F. P. Chavez, and A. Paytan. 2007. Nitrification in the euphotic zone as evidenced by nitrate dual isotopic composition: Observations from Monterey Bay, California. Glob. Biogeochem. Cycles **21:** GB2009, doi:10.1029/2006GB002723

Ward, B. B. 2008. Nitrification in marine systems, p. 199–262. *In* D. G. Capone, D. Bronk, M. Mulholland, and E. J. Carpenter [eds.], Nitrogen in the marine environment, 2nd ed. Academic.

———, H. E. Glover, and F. Lipschultz. 1989*a*. Chemoautotrophic activity and nitrification in the oxygen minimum zone off Peru. Deep-Sea Res. A **36:** 1031–1051, doi:10.1016/0198-0149(89)90076-9

———, K. A. Kilpatrick, E. H. Renger, and R. W. Eppley. 1989*b*. Biological nitrogen cycling in the nitracline. Limnol. Oceanogr. **34:** 493–513, doi:10.4319/lo.1989.34.3.0493

———, and O. C. Zafiriou. 1988. Nitrification and nitric oxide in the oxygen minimum of the eastern tropical North Pacific. Deep-Sea Res. A **35:** 1127–1142, doi:10.1016/0198-0149(88)90005-2

———, and others. 2009. Denitrification as the dominant nitrogen loss process in the Arabian Sea. Nature **461:** 78–81, doi:10.1038/nature08276

White, A. E., F. G. Prahl, R. M. Letelier, and B. N. Popp. 2007. Summer surface waters in the Gulf of California: Prime habitat for biological N_2 fixation. Glob. Biogeochem. Cycles **21:** GB2017, doi:10.1029/2006GB002779

Yool, A., A. P. Martin, C. Fernandez, and D. R. Clark. 2007. The significance of nitrification for oceanic new production. Nature **447:** 999–1002, doi:10.1038/nature05885

Associate Editor: Bo Thamdrup

Received: 27 May 2011
Accepted: 26 January 2012
Amended: 01 February 2012